Nuclear fission modes and fragment mass asymmetries in a five-dimensional deformation space

P. Möller*, D. G. Madland*, A. J. Sierk* & A. Iwamoto†

** Theoretical Division, Los Alamos National Laboratory, Los Alamos, New Mexico 87545, USA*
† Department of Materials Science, Japan Atomic Energy Research Institute, Tokai-mura, Naka-gun, Ibaraki, 319-1195 Japan

Nuclei undergoing fission can be described by a multi-dimensional potential-energy surface that guides the nuclear shape evolution—from the ground state, through intermediate saddle points and finally to the configurations of separated fission fragments. Until now, calculations have lacked adequate exploration of the shape parameterization of sufficient dimensionality to yield features in the potential-energy surface (such as multiple minima, valleys, saddle points and ridges) that correspond to characteristic observables of the fission process. Here we calculate and analyse five-dimensional potential-energy landscapes based on a grid of 2,610,885 deformation points. We find that observed fission features—such as the distributions of fission fragment mass and kinetic energy, and the different energy thresholds for symmetric and asymmetric fission—are very closely related to topological features in the calculated five-dimensional energy landscapes.

When a heavy nucleus divides into two fragments in nuclear fission, two key questions about the process have challenged researchers since the discovery of fission more than 60 years ago. First, what is the threshold energy for the reaction and, second, what shape changes are involved in the transition from a single nuclear system to two separated daughter fragment nuclei? These two questions are intimately connected. The potential energy of a nucleus as a function of shape defines a landscape in a multi-dimensional deformation space. In this landscape, the energy of the lowest mountain passes, or saddle points, connecting the nuclear ground state with the region corresponding to separated fragments, represents the threshold energy of the fission process.

Previous theories and results

The first theory of fission, put forward in 1939 by Meitner and Frisch[1] and Bohr and Wheeler[2], explained the break-up of uranium into two lighter fragments of roughly equal size with a model involving a charged liquid drop with surface tension. This break-up had been observed just months earlier by Hahn and Strassmann[3] in the reaction n + U. In such a macroscopic model the drop becomes increasingly less stable with respect to deformation when the atomic number Z increases, and at $Z \approx 100$ stability is completely lost. For slightly lighter actinide nuclei the fission barrier between the ground-state shape and the separated-fragment configuration is sufficiently low that spontaneous fission, due to quantum-mechanical penetration of the fission barrier, occurs with measurable probability. Fission may also be induced by exciting the nucleus to energies above the barrier energy. For example, a thermal neutron incident upon ^{235}U imparts sufficient energy to excite the compound nucleus ^{236}U above the barrier.

In a pioneering use of the first electronic digital computer ENIAC in 1947, Frankel and Metropolis[4] explored some key aspects of the macroscopic liquid-drop model. In particular, they determined the shapes of fissioning nuclei at the saddle-point thresholds. In the 1960s a greatly improved model for the nuclear potential energy as a function of shape emerged. In this macroscopic–microscopic model, the potential energy is the sum of shape-dependent macroscopic (liquid-drop) and microscopic (single-particle) terms. Over the past 30 years the model has provided considerable insight into nuclear structure. For example, improved descriptions of fission-isomeric states and mass-asymmetric fission saddle points have been obtained and nuclear masses are calculated for nuclei throughout the periodic system to an average root-mean-square (r.m.s.) accuracy of about 0.7 MeV (refs 5–13).

The microscopic energy, calculated by following the method developed by Strutinsky[5,6] and representing a modification to the slowly varying macroscopic 'liquid drop' energy of the nucleus, is due to the presence of quantum-mechanical structure in the nucleus. For chemical properties it is well known that certain elements, the noble gases, are unusually stable and non-reactive, due to particularly stable electron configurations, which occur for 2, 10, 18, 36, 54 and 86 electrons, corresponding to He, Ne, Ar, Kr, Xe and Rn. At these numbers large gaps occur in the energy-level spectrum corresponding to the individual electron orbitals. In nuclei, quantum-mechanical laws give rise to increased stability at similar gaps corresponding to nuclear 'magic numbers' for protons and neutrons. Because of differences between the purely electromagnetic forces determining the electron levels and the nuclear forces, the first few 'magic numbers' for spherical nuclei are 2, 8, 20, 28, 50 and 82 for both protons and neutrons. However, although the effects are largest for the 'magic' nuclei, microscopic corrections to the simple liquid-drop model of nuclei occur to some degree in all nuclei. Strutinsky[5,6] generalized the concept of magic numbers so that a precise, well specified microscopic (shell) correction to the liquid-drop energy can be calculated for any shape and any particle number. It is the shell-correction part of the total nuclear energy that is responsible for the multiple valleys, minima, saddle points and peaks that appear in general multi-dimensional potential-energy surfaces as functions of nuclear shape. In such surfaces it has been demonstrated, for some nuclei in limited shape parameterizations, that 'shells' or regions of unusually low energy corresponding to magic numbers in separated fission fragments manifest themselves as deep valleys in the nuclear potential energy surface long before division into separate daughter fragments[14–17]. However, to what extent ridges stabilize these valleys was unclear in these previous, lower dimensional, schematic calculations.

In the past, fission properties have often been correlated with models of the binding energy of separated fission fragments, and of valleys inside the point of contact. However, the valleys by

themselves do not determine the final state of a fissioning nucleus. Final states corresponding to three or more fragments are in many cases energetically more favoured than are states of two final fission fragments. In these cases the nucleus nonetheless divides into only two fragments. This occurs because the barrier between the ground state and the binary fission valley favours such divisions and a ridge separates the binary from the ternary valley, although dynamical effects may also affect the division. Here we examine what saddles connect the ground state to the various two-fragment valleys that emerge in the later stages of the fission process, and what are the heights of the ridges that allow or prevent movement between the valleys.

Unsolved mysteries

With our new approach we are now able to explain a number of previously unresolved, very important characteristic features of fission. These include:

(1) Nuclei just below the actinide region close to ^{228}Ra exhibit two fission modes[18–21]. Figure 1 illustrates experimental data obtained for ^{227}Ra in ref. 19. In one mode, with the lower threshold energy, the fragment mass distribution is asymmetric and the total fragment kinetic energy is about 10 MeV higher than in the other, symmetric, mode[19]. At certain excitation energies these two modes lead to a striking three-peaked structure of the fragment-mass yield curve. From the totality of the experimental data the authors of ref. 19 conclude: "Thus it seems that after the gross determination of the symmetric or asymmetric character of fission made already at the barrier, the two components follow a different path with no or little overlap in the development from the barrier to the scission configuration."

(2) Nuclei at the upper end of the actinide region exhibit sudden changes with nucleon number in fission properties and sometimes display a two-mode character in the same nucleus. For example, the fragment mass distribution changes abruptly from mass asymmetric for ^{256}Fm to mass symmetric for ^{258}Fm along with a correlated increase in the fragment total kinetic energy (TKE) by about 35 MeV. But ^{258}Fm also exhibits the asymmetric mode with lower TKE with a small probability: fission of such nuclei is characterized as bimodal.

(3) Throughout the actinide region below Fm, nuclei near the line of β-stability in spontaneous or low-energy induced fission divide into a heavy fragment with a mass close to 140 and a light fragment with a mass that shifts with the total mass of the fissioning nucleus. An example of a typical fission-fragment charge (mass) distribution is shown in Fig. 2. In our new strategy for applying the macroscopic–microscopic method to higher-dimensional spaces, all of these observed fission phenomena can be understood in terms of nuclear potential-energy surfaces calculated with five appropriately chosen nuclear shape degrees of freedom.

New approach

Since the early 1970s (refs 5–11), there has been no major improvement in the description of the fission potential-energy landscape, although many calculations based on 1,000 or so points in deformation space have been presented. We have learned that to describe properly the evolution of a single nuclear shape into two fragments of different mass and deformation—for example, one spherical ^{132}Sn-like fragment and one deformed fragment with mass number A near 100—at least five independent shape parameters are required. Earlier, approaches such as self-consistent Hartree–Fock calculations (see discussion in ref. 22) constrained with respect to one variable were sometimes thought to take into account automatically all additional shape degrees of freedom. In other approaches, also called multi-dimensional, the calculated energy was displayed as energy contour maps in terms of two shape degrees of freedom where the energy at each point was minimized with respect to additional shape coordinates. Neither approach results in a correct description of the structure of the full, multi-dimensional fission potential-energy surface. In fact, they are at least as inexact as two-dimensional calculations, as is discussed in more detail in ref. 22. To establish the structure of multi-dimensional spaces it is necessary to calculate the energies corresponding to all physically possible combinations of the deformation parameters, which leads to multi-million-point potential-energy spaces rather than only 1,000 or so points.

We investigate in detail such a space incorporating 2,610,885 points defining a five-dimensional shape-coordinate grid. For the potential energy we use the macroscopic–microscopic finite-range liquid-drop model with shape-dependent Wigner and A^0 terms as defined in refs 12 and 16. Specifically the five shape coordinates are: (1) elongation, expressed in terms of the charge quadrupole moment Q_2; (2) neck diameter d; (3) left nascent-fragment deformation ϵ_{f1}; (4) right nascent-fragment deformation ϵ_{f2}; and (5) mass asymmetry α_g, as illustrated in Fig. 3. The charge quadrupole moment Q_2 is given as that of ^{240}Pu with the same shape as the nucleus being considered, so that the nuclear size effect is

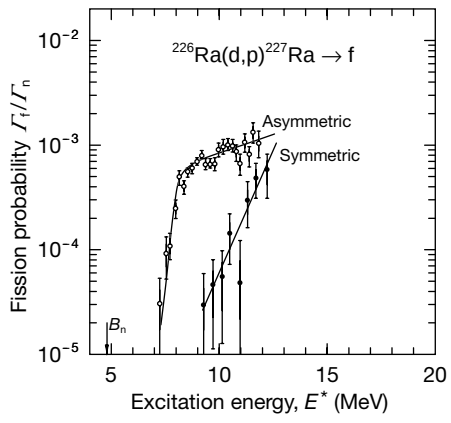

Figure 1 Asymmetric and symmetric fission probabilities for ^{227}Ra as functions of the excitation energy in the fissioning nucleus. Here d denotes a deuteron, p a proton, B_n the neutron binding energy, and Γ_n and Γ_f are proportional to the neutron-emission and fission probabilities, respectively. The data show that two distinct fission modes coexist in this nucleus, namely one asymmetric mode and one symmetric mode, the latter with a 1–2 MeV higher threshold energy. The figure is based on a figure in ref. 19.

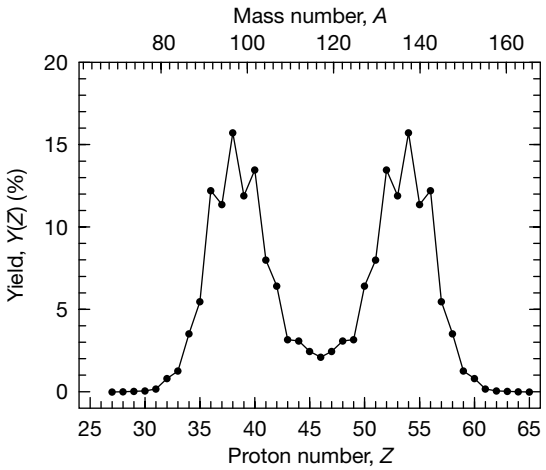

Figure 2 Nuclear charge yield in electromagnetic-induced fission of ^{234}U from ref. 28. The data are converted to a mass–yield distribution before neutron emission (top axis) by assuming that the proton/neutron ratio Z/N is the same in each of the two fission fragments as in the original nucleus.

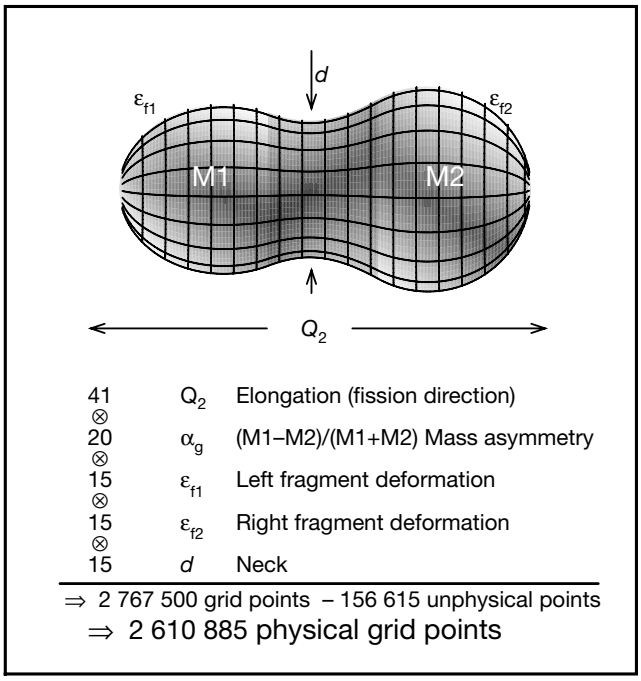

Figure 3 Five-dimensional shape parameterization used in our potential-energy calculation. Different shades of grey indicate the three different quadratic surfaces of the shape parameterization used in our calculation. The first derivative is continuous at the intersections of the surfaces. The crossed circles indicate that the five one-dimensional spaces of each coordinate combine (multiply together) to yield a five-dimensional space with 2,767,500 grid points. However, shapes corresponding to certain quadrupole moments do not exist for specific combinations of the other shape parameters. For example, zero quadrupole moment cannot be realized for shapes with very deformed ends. In our grid there exist 156,615 such 'unphysical' points. Thus, we are left with 2,610,885 shapes for which we actually calculate the potential energy. We have closely spaced the asymmetry coordinate so that we will be able to identify favourable saddle-point shapes, close to fragment magic proton and neutron numbers, that may not appear in a more sparsely spaced grid. For ^{240}Pu the spacing corresponds to a change of 2.4 units in the nascent fragment mass numbers.

eliminated. The end-body masses (or, equivalently, volumes) M_1 and M_2 are the masses of the left and right nascent fragments were they completed to closed shapes. The nascent fragments are partial spheroids whose deformations we characterize by Nilsson's quadrupole ϵ parameter[7]. They are smoothly joined by a partial spheroid or hyperboloid of revolution. Our approach is based on an established realistic microscopic interaction[12,23], and the energy behaves properly as the shape evolves from the one limit of a single shape corresponding to the nuclear ground state to the other limit of scission configurations corresponding to two touching daughter fission fragments. By 'properly' we mean that the model is formulated so that for a touching-fragment configuration we obtain the same energy whether the energy is calculated as that of a single, very deformed nucleus or as that of two touching nuclei[16].

We identify significant structures in the calculated five-dimensional potential-energy space by considering imaginary water flows[24] in five dimensions[22]. The threshold saddle-point energy and the corresponding shape are found by tracing this imaginary water flow across saddle points when various minima are gradually filled with water.

Given the determination of the threshold energies for fission and the nuclear shapes corresponding to the saddle-point locations, we turn to the second key question: what are the shape changes involved in the transition from a single nucleus to two separated daughter fragment nuclei? Do structures exist in the potential-energy surface that lead to multi-mode fission such as that of the well known three-peaked mass distribution in ^{228}Ra fission[19]? To look for such structures we ask whether there are valleys of distinctly different character running in the fission direction of increasing Q_2. That is, for ten or more fixed Q_2 values beyond the outer saddle region, we determine all minima in the remaining four-dimensional space of the two fragment deformations, neck size and mass asymmetry. We find that there are usually two (but sometimes more) distinct valleys in the region beyond the second saddle region, one corresponding to a mass asymmetry α_g of about $[140 - (A - 140)]/A$ and one corresponding to mass symmetry $\alpha_g = 0$. To understand the significance of these valleys it is necessary to determine more details about their interconnections in the five-dimensional deformation-energy space.

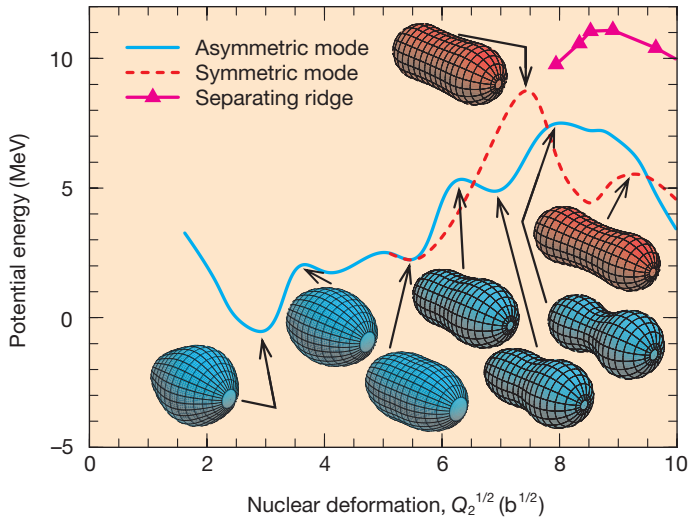

Figure 4 Calculated potential-energy valleys and ridges and corresponding nuclear shapes for ^{228}Ra. Two fission paths exist: one asymmetric path and one symmetric path. The symmetric path has a higher fission saddle point and the more elongated shapes in the valley beyond the saddle point indicate that total fragment kinetic energies in the symmetric mode are lower than in the asymmetric mode. For excitation energies just above the symmetric saddle the ridge separating the two valleys is high enough to keep the two modes well separated.

Variations of the flooding algorithm allow us to determine that separate saddle points provide entries to the two valleys and the respective energies of these saddle points. Once the lowest saddle has been determined we may block the water flow across this saddle by building an imaginary dam across the saddle region. We can also totally block the water flow beyond a selected maximum Q_2. This prevents water from flowing down one valley and up 'the back way' into the other valley. To determine the height of the ridge between the two valleys along their entire length, for each fixed Q_2, we study the remaining four-dimensional space in which the two valleys correspond to two minima and the ridge to the saddle separating them. We use the flooding algorithm in four dimensions to localize this saddle/ridge.

Mysteries resolved

As examples of structures we have found in the calculated five-dimensional potential-energy surfaces we show in Figs 4 and 5 some fission-valley and separating-ridge features obtained for ^{228}Ra and ^{234}U. Asymmetric fission dominates in both cases, because the barrier leading into the asymmetric valley is the lower one, in agreement with experiment. At the saddle points leading to the asymmetric fission valleys the shell correction is already about half of the one calculated for the spherical ground-state shape of ^{132}Sn, whereas the shell correction at the saddle points leading to the symmetric fission valleys is essentially zero. The calculated bi-valley structure of the potential-energy surface leads to the observed bimodal fission features in this region of nuclei[19,21]. The high ridge separating the two valleys for ^{228}Ra peaks at 2.47 MeV above the

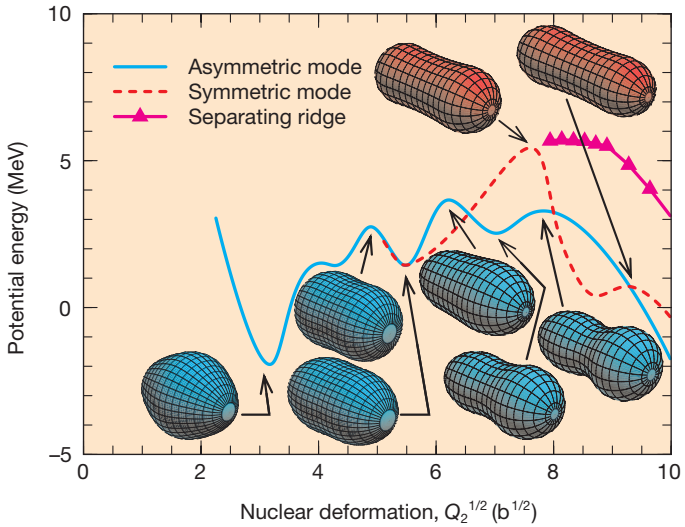

Figure 5 Calculated potential-energy valleys and ridges and corresponding nuclear shapes for ^{234}U. Two fission paths exist: one asymmetric path and one symmetric path. The symmetric path has a higher fission saddle point and the more elongated shapes in the valley beyond the saddle point indicate that total fragment kinetic energies in the symmetric mode are lower than in the asymmetric mode. The ridge separating the two valleys is certainly not high enough to permit two well-separated modes to evolve.

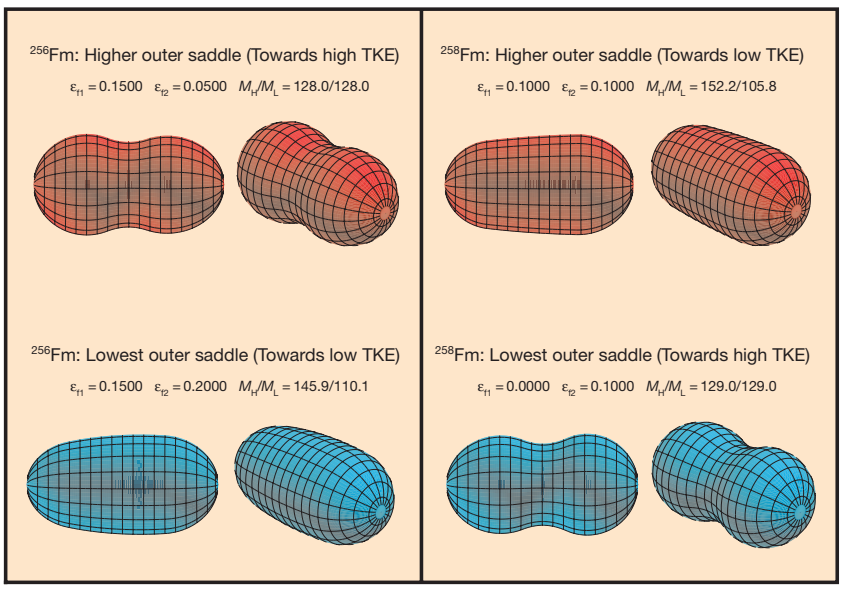

Figure 6 Several saddle-point shapes for ^{256}Fm and ^{258}Fm calculated on the grid in ref. 22. Two views are plotted for each calculated shape; a side view and a view from an angle. For ^{258}Fm the lowest saddle-point energy corresponds to a compact, mass-symmetric shape configuration, which with its nearly spherical nascent fragments corresponds to the experimental observation of high fission-fragment kinetic energies and mass-symmetric fission. An observed weak mode of low-kinetic-energy fission corresponds to fission in a valley accessible across the higher calculated saddle in the top right part of the figure. For ^{256}Fm the calculated heights of these two saddles are reversed, favouring both low fission-fragment kinetic energies and fragment mass asymmetry, in agreement with the experimental observations. TKE stands for total kinetic energy.

entrance saddle to the symmetric valley. At low excitation energies it therefore keeps the mass-symmetric and mass-asymmetric modes well separated until scission, whereas for ^{234}U the lower separating ridge, at almost the same energy as the entrance saddle to the symmetric valley, allows the symmetric component to partially or completely revert back to the asymmetric valley before scission. The elongated shapes obtained in the symmetric valley are consistent with the lower fragment kinetic energies observed in the symmetric fission mode relative to the asymmetric mode for which we obtain more compact shapes. The fragment kinetic energies arise from Coulomb repulsion which mainly becomes effective just after division into separated fragments. The centres of charge of more elongated touching fragments are farther apart than for compact touching fragments. High fragment kinetic energies therefore indicate compact scission configurations, whereas low fragment kinetic energies indicate more elongated scission configurations.

Nuclei in the region near ^{258}Fm also exhibit bimodal fission features[25]. We have earlier tentatively identified bimodal structures in calculated two-dimensional potential-energy surfaces[15,16], but only now have we verified that these interpretations remain valid when the calculation is extended from two to five dimensions. For ^{256}Fm and ^{258}Fm we find the two distinct classes of saddle points shown in Fig. 6. For ^{256}Fm the shape of the lowest saddle indicates it corresponds to normal, low-TKE fission similar to what is observed in fission of lighter actinides. However, another saddle point exists, which we calculate to be 0.30 MeV higher than the lower saddle point. This saddle-point shape shows that it corresponds to a path leading to symmetric fission with compact scission configurations and higher fragment kinetic energies. For ^{258}Fm the latter type of saddle point is the lowest saddle point. Thus, we reproduce the experimentally observed transition point between asymmetric low-TKE fission and symmetric high-TKE fission[25].

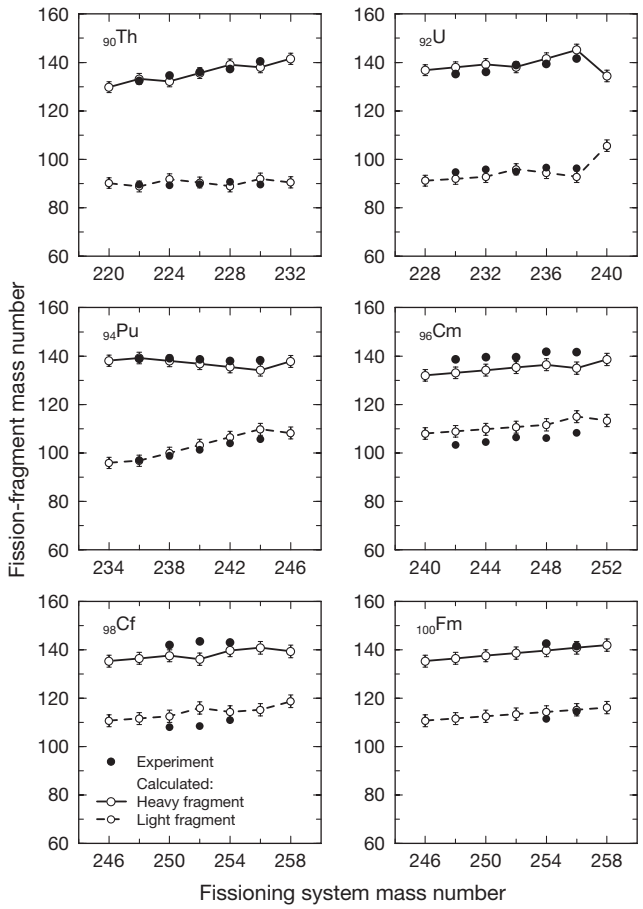

Figure 7 Calculated (white circles) and measured (black circles)[26–28] average mass division in asymmetric fission for sequences of even isotopes of Th, U, Pu, Cm, Cf, and Fm. The error bars on the calculated points correspond to the spacing of mass asymmetry values on the multidimensional shape-coordinate grid. The data are for spontaneous fission when they are available, otherwise data for low-energy induced fission are used. The results reproduce the experimental observation of a heavy fragment at mass number $A \approx 140$ and a light fragment with mass corresponding to the remainder of the original nucleus. However, deviations from this rule of thumb are also reproduced by the calculations.

For elongations between the outer fission-barrier saddle point and scission we can unambiguously identify a mass-asymmetric valley for most actinide nuclei. We have defined the deformation-grid mass-asymmetry parameter α_g (compare Fig. 3) as

$$\alpha_g = \frac{M_1 - M_2}{M_1 + M_2} \quad (1)$$

where M_1 and M_2 are the volumes inside the end-body quadratic surfaces, were they completed to form closed-surface spheroids. Sufficiently far along in the mass-asymmetric valley, say at $Q_2 = 64$ b, where 1b is 1 barn, corresponding to 10^{-28} m^2, the fissioning nuclei always have well-developed necks (see Figs 4 and 5). Therefore it is meaningful to compare the mass asymmetry of the non-separated shape in the mass-asymmetric valley to the final heavy and light fragment masses M_H and M_L.

Although M_1 and M_2 for shapes with well-developed necks can be expected to be close to the final fragment masses we cannot directly compare M_1 and M_2 to the observed fission fragment masses M_H and M_L because the former do not quite sum up to the total nuclear volume or mass A. However, by scaling M_1 and M_2 so that their sum adds up to the total mass number A, we can directly compare the mass asymmetry of the valley shape to the observed heavy and light fragment masses. We obtain trivially

$$M_L^{calc} = r_s M_1 = A\frac{1+\alpha_g}{2}, \quad M_H^{calc} = r_s M_2 = A\frac{1-\alpha_g}{2}$$
$$\text{and} \quad r_s = \frac{A}{M_1 + M_2} \quad (2)$$

where r_s is a scaling factor for a nucleus with A nucleons. The scaling is equivalent to a redistribution of the mass in the neck region to the left and right masses in proportion to their respective volumes. The amount of matter in this 'gedanken' redistribution is quite small, about 10–20 nucleons.

We use the above definitions in Fig. 7 to compare calculated heavy and light fission-fragment masses, based on valley properties at $Q_2 = 99$ b, to experimental data for the mean positions of the heavy- and light-mass peaks in fragment-mass distributions[26–28] for a range of even isotopes of Th, U, Pu, Cm, Cf and Fm. Our calculated results are in excellent agreement with experimental data, with a mean deviation of only 3.0 nucleons. Specifically, we find that the calculated heavy-fragment mass is roughly constant and close to $A = 140$ for all elements and all isotopes considered. Consequently the mass of the light fragment, which contains the remainder of the mass of the fissioning nucleus, depends on the mass number of the fissioning system, again in excellent agreement with experimental data.

Discussion

The new theoretical results on nuclear fission presented here have been obtained in our standard nuclear-structure model[29,30] that has also been applied to the calculation of nuclear masses[12], heavy-ion interaction barriers[31], nuclear β-decay[32], and nucleosynthesis in stellar environments[33], with no change in the model or its parameters relative to their 1992 definitions in ref. 12. We have used the FRLDM (1992) version[12] of the potential-energy model, rather than the FRDM (1992) version[12] because the latter is unsuitable for shapes with well-developed necks. We have calculated five-dimensional potential-energy landscapes for 138 even–even nuclei from

Pb to Fm. Our analysis of these landscapes, of which only some examples have been discussed in detail above, allows us to draw the following conclusions:
(1) Multiple fission paths are found for most nuclei.
(2) For radium and light actinide nuclei two paths dominate: one mass asymmetric and one mass symmetric. These paths correspond to different fission modes, such as those illustrated in Fig. 1.
(3) The difference in energy between the symmetric and asymmetric saddle points for Ra and light actinide nuclei in our calculated potential-energy surfaces is 1–2 MeV, which is consistent with the experimentally inferred differences in threshold energies for these two modes[19–21,34].
(4) For ^{228}Ra and nearby nuclei we find that the symmetric and asymmetric fission paths are well separated by a high ridge from saddle to scission. Thus, our five-dimensional calculations have verified the experimental conclusion reached in ref. 19 that at low excitation energies two fission paths exist with little or no overlap.
(5) From experimental observations of fission of elements lighter than Fm it is deduced that the average kinetic energy is 10–15 MeV higher for the asymmetric mode than for the symmetric mode[18,19,35]. The shape differences we calculate for nuclei evolving in the mass-asymmetric and mass-symmetric valleys are qualitatively consistent with these differences in the kinetic energies of the two modes.
(6) The saddle-point shapes and energies for ^{256}Fm and ^{258}Fm are consistent with the experimentally observed transition between asymmetric low-TKE fission and symmetric high-TKE fission that occurs between ^{256}Fm and ^{258}Fm.
(7) The long-observed mass split in mass-asymmetric fission with a roughly constant heavy fragment mass near $A = 140$ is convincingly reproduced in our calculations.

As early as 1950 Meitner[36] suggested an interpretation of the observed mass divisions in fission in terms of fragment shell structure. We have shown here that it is not only the mass division that is influenced by shell structure. Shell structure also creates different modes of fission, each of which has its characteristic saddle-point energy, mass division, and kinetic energy.

The five-dimensional fission potential-energy surface at and beyond the several outer saddle points is an imposing landscape traversed by deep valleys and high ridges. The fragment shells profoundly influence the topography of this landscape, long before the system divides into separated fission fragments.

Note added in proof: An interesting discussion of the problem of finding structures in multidimensional spaces is in ref. 37. □

Received 3 August; accepted 18 December 2000.

1. Meitner, L. & Frisch, O. R. Disintegration of uranium by neutrons: A new type of nuclear reaction. *Nature* **143,** 239–240 (1939).
2. Bohr, N. & Wheeler, J. A. The mechanism of fission. *Phys. Rev.* **56,** 426–450 (1939).
3. Hahn, O. & Strassmann, F. Über den Nachweiss und das Verhalten der bei der Bestrahlung des Urans mittels Neutronen entstehenden Erdalkalimetalle. *Naturwissenschaften* **27,** 11–15 (1939).
4. Frankel, S. & Metropolis, N. Liquid-drop model of fission. *Phys. Rev.* **72,** 914–925 (1947).
5. Strutinsky, V. M. Shell effects in nuclear masses and deformation energies. *Nucl. Phys. A* **95,** 420–442 (1967).
6. Strutinsky, V. M. Shells in deformed nuclei. *Nucl. Phys. A* **122,** 1–33 (1968).
7. Nilsson, S. G. *et al.* On the nuclear structure and stability of heavy and superheavy elements. *Nucl. Phys. A* **131,** 1–66 (1969).
8. Pashkevich, V. V. The energy of non-axial deformation of heavy nuclei. *Nucl. Phys. A* **133,** 400–404 (1969).
9. Möller, P. & Nilsson, S. G. The fission barrier and odd-multipole shape distortions. *Phys. Lett.* **31B,** 283–286 (1970).
10. Brack, M. *et al.* Funny hills: The shell-correction approach to nuclear shell effects and its applications to the fission process. *Rev. Mod. Phys.* **44,** 320–405 (1972).
11. Nix, J. R. Calculation of fission barriers for heavy and superheavy nuclei. *Annu. Rev. Nucl. Sci.* **22,** 65–120 (1972).
12. Möller, P., Nix, J. R., Myers, W. D. & Swiatecki, W. J. Nuclear ground-state masses and deformations. *Atom. Data Nucl. Data Tables* **59,** 185–381 (1995).
13. Aboussir, Y., Pearson, J. M., Dutta, A. K. & Tondeur, F. Nuclear-mass formula via an approximation to the Hartree-Fock method. *Atom. Data Nucl. Data Tables* **61,** 127–176 (1995).
14. Möller, P. & Nix, J. R. Potential-energy surfaces for asymmetric heavy-ion reactions. *Nucl. Phys. A* **281,** 354–372 (1977).
15. Möller, P., Nix, J. R. & Swiatecki, W. J. Calculated fission properties of the heaviest elements. *Nucl. Phys. A* **469,** 1–50 (1987).
16. Möller, P., Nix, J. R. & Swiatecki, W. J. New developments in the calculation of heavy-element fission barriers. *Nucl. Phys. A* **492,** 349–387 (1989).
17. Armbruster, P. Nuclear structure in cold rearrangement processes in fission and fusion. *Rep. Prog. Phys.* **62,** 465–525 (1999).
18. Britt, H. C., Wegner, H. E. & Gursky, J. C. Energetics of charged particle-induced fission reactions. *Phys. Rev.* **129,** 2239–2252 (1963).
19. Konecny, E., Specht, H. J. & Weber, J. in *Proc. Third IAEA Symp. Phys. Chem. Fission* Vol. II, 3–18 (International Atomic Energy Agency, Vienna, 1974).
20. Ohtsuki, T., Nakahara, H. & Nagame, Y. Systematic variation of fission barrier heights for symmetrical and asymmetric mass divisions. *Phys. Rev. C* **48,** 1667–1676 (1993).
21. Nagame, Y. *et al.* Bimodal nature of low energy fission of light actinides. *Radiochim. Acta* **78,** 3–10 (1997).
22. Möller, P. & Iwamoto, A. Realistic fission saddle-point shapes. *Phys. Rev. C* **61,** 47602-1–4 (2000).
23. Möller, P., Nix, J. R. & Kratz, K.-L. Nuclear properties for astrophysical and radioactive-ion-beam applications. *Atom. Data Nucl. Data Tables* **66,** 131–343 (1997).
24. Mamdouh, A., Pearson, J. M., Rayet, M. & Tondeur, F. Large-scale fission-barrier calculations with the ETFSI method. *Nucl. Phys. A* **644,** 389–414 (1998).
25. Hulet, E. K. *et al.* Bimodal symmetrical fission observed in the heaviest elements. *Phys. Rev. Lett.* **56,** 313–316 (1986).
26. Hoffman, D. C. & Hoffman, M. M. Post-fission phenomena. *Annu. Rev. Nucl. Sci.* **24,** 151–207 (1974).
27. Dematte, L., Wagemans, C., Barthelemy, R., Dhondt, P. & Deruytter, A. Fragments' mass and energy characteristics in the spontaneous fission of Pu-236, Pu-238, Pu-240, Pu-242 and Pu-244. *Nucl. Phys. A* **617,** 331–346 (1997).
28. Schmidt, K.-H. *et al.* Relativistic radioactive beams: A new access to nuclear-fission studies. *Nucl. Phys. A* **665,** 221–267 (2000).
29. Bolsterli, M., Fiset, E. O., Nix, J. R. & Norton, J. L. New calculation of fission barriers for heavy and superheavy nuclei. *Phys. Rev. C* **5,** 1050–1075 (1972).
30. Krappe, H. J., Nix, J. R. & Sierk, A. J. Unified nuclear potential for heavy-ion elastic scattering, fusion, fission, and ground-state masses and deformations. *Phys. Rev. C* **20,** 992–1013 (1979).
31. Möller, P. & Iwamoto, A. Macroscopic potential-energy surfaces for arbitrarily oriented, deformed heavy-ions. *Nucl. Phys. A* **575,** 381–411 (1994).
32. Möller, P. & Randrup, J. New developments in the calculation of β-strength functions. *Nucl. Phys. A* **514,** 1–48 (1990).
33. Kratz, K.-L., Bitouzet, J.-P., Thielemann, F.-K., Möller, P. & Pfeiffer, B. Isotopic r-process abundances and nuclear-structure far from stability: implications for the r-process mechanism. *Astrophys. J.* **403,** 216–238 (1993).
34. Kudyaev, G. A., Ostapenko, Yu. B. & Smirenkin, G. N. Thresholds and saddle shapes in symmetric and asymmetric fission in the vicinity of Ra. *Sov. J. Nucl. Phys.* **45,** 951–958 (1987).
35. Zhao, Y. L. *et al.* Experimental verification of two deformation paths in the mass division process of actinides. *J. Alloys Comp.* **271,** 327–330 (1998).
36. Meitner, L. Fission and nuclear shell model. *Nature* **165,** 561 (1950).
37. Hayes, B. Dividing the continent. *Am. Sci.* **88,** 481–485 (2000).

Acknowledgements

The calculations on which the results in this paper are based were carried out on the cluster of 4 Alpha processors at the TANDEM accelerator in JAERI in the winter of 1998–99 and subsequently on the AVALON cluster of 140 Alpha processors at Los Alamos. This research is supported by the US DOE.

Correspondence and requests for materials should be addressed to P.M. (e-mail: moller@moller.lanl.gov).